Phenoxyl radicals: H-bonded and coordinated to Cu(II) and Zn(II)†

Laurent Benisvy,*[a] Eckhard Bill,[b] Alexander J. Blake,[a] David Collison,[c] E. Stephen Davies,[a] C. David Garner,*[a] Graeme McArdle,[a] Eric J. L. McInnes,[c] Jonathan McMaster,*[a] Stephanie H. K. Ross[a] and Claire Wilson[a]

Received 16th September 2005, Accepted 14th October 2005
First published as an Advance Article on the web 9th November 2005
DOI: 10.1039/b513221p

Two pro-ligands (^{R}LH) comprised of an *o*,*p*-di-*tert*-butyl-substituted phenol covalently bonded to a benzimidazole (^{Bz}LH) or a 4,5-di-*p*-methoxyphenyl substituted imidazole (^{PhOMe}LH), have been structurally characterised. Each possesses an intramolecular O–H ⋯ N hydrogen bond between the phenolic O–H group and an imidazole nitrogen atom and ^{1}H NMR studies show that this bond is retained in solution. Each ^{R}LH undergoes an electrochemically reversible, one-electron, oxidation to form the [^{R}LH]$^{\bullet+}$ radical cation that is considered to be stabilised by an intramolecular O ⋯ H–N hydrogen bond. The ^{R}LH pro-ligands react with $M(BF_4)_2{\cdot}H_2O$ (M = Cu or Zn) in the presence of Et_3N to form the corresponding [M(^{R}L)$_2$] compound. [Cu(^{Bz}L)$_2$] (**1**), [Cu(^{PhOMe}L)$_2$] (**2**), [Zn(^{Bz}L)$_2$] (**3**) and [Zn(^{PhOMe}L)$_2$] (**4**) have been isolated and the structures of **1**·4MeCN, **2**·2MeOH, **3**·2MeCN and **4**·2MeCN determined by X-ray crystallography. In each compound the metal possesses an N_2O_2-coordination sphere: in **1**·4MeCN and **2**·2MeOH the $\{CuN_2O_2\}$ centre has a distorted square planar geometry; in **3**·2MeCN and **4**·2MeCN the $\{ZnN_2O_2\}$ centre has a distorted tetrahedral geometry. The X-band EPR spectra of both **1** and **2**, in CH_2Cl_2–DMF (9 : 1) solution at 77 K, are consistent with the presence of a Cu(II) complex having the structure identified by X-ray crystallography. Electrochemical studies have shown that **1**, **2**, **3** and **4** each undergo two, one-electron, oxidations; the potentials of these processes and the UV/vis and EPR properties of the products indicate that each oxidation is ligand-based. The first oxidation produces [M(II)(^{R}L)(^{R}L$^{\bullet}$)]$^{+}$, comprising a M(II) centre bound to a phenoxide (^{R}L) and a phenoxyl radical (^{R}L$^{\bullet}$) ligand; these cations have been generated electrochemically and, for R = PhOMe, chemically by oxidation with $Ag[BF_4]$. The second oxidation produces [M(II)(^{R}L$^{\bullet}$)$_2$]$^{2+}$. The information obtained from these investigations shows that a suitable pro-ligand design allows a relatively inert phenoxyl radical to be generated, stabilised by either a hydrogen bond, as in [^{R}LH]$^{\bullet+}$ (R = Bz or PhOMe), or by coordination to a metal, as in [M(II)(^{R}L)(^{R}L$^{\bullet}$)]$^{+}$ (M = Cu or Zn; R = Bz or PhOMe). Coordination to a metal is more effective than hydrogen bonding in stabilising a phenoxyl radical and Cu(II) is slightly more effective than Zn(II) in this respect.

Introduction

Tyrosyl radicals play vital roles in the chemistry of living systems.[1,2] At least three different environments have been established for a tyrosyl radical within a metalloprotein: (i) "free", *e.g.* Tyr_{122} of the iron-dependent ribonucleotide reductase (RNR) from *Escherichia coli*;[1–3] (ii) hydrogen-bonded to an adjacent histidine residue, *e.g.* the Tyr_D-His_{189} moiety of photosystem II (PSII);[1,4] and (iii) co-ordinated to a Cu^{II} centre, as in the active form of galactose oxidase (GO).[1,5,6] The potential of the Tyr$^{\bullet}$/Tyr redox couple is modulated by the protein environment, *e.g.* the value (*vs.* NHE) varies as: 1.00 ± 0.10 V for Tyr_{122} in RNR (pH 7.6);[3] 0.72–0.76 V for Tyr_D in PSII (pH ~6.0);[4] and 0.40 V for Tyr_{272} in GO (pH 7.5),[6] the potential produced being compatible with the function of the particular Tyr$^{\bullet}$/Tyr couple. The factors that determine the properties of a hydrogen-bonded or a metal-bonded phenoxyl radical remain to be defined; this challenge has attracted considerable attention and has led to the synthesis and investigation of chemical systems that contain a phenoxyl radical stabilised by an intramolecular hydrogen bond[7–12] or bound to a metal centre.[11–15]

We have reported the synthesis of a new family of pro-ligands, ^{R}LH (R = Ph, PhOMe or Bz) (Scheme 1)[11,15] each of which comprises an imidazole group covalently bonded to an *o*,*p*-di-*tert*-butyl-substituted phenol. The crystal structure of ^{Ph}LH identified an intramolecular hydrogen bond between the phenolic

[a]*School of Chemistry, The University of Nottingham, University Park, Nottingham, UK NG7 2RD. E-mail: Dave.Garner@nottingham.ac.uk*
[b]*Max-Planck-Institut für Bioanorganische Chemie, Stiftstrasse 34-46, Mülheim an der Ruhr, D-45470, Germany*
[c]*School of Chemistry, The University of Manchester, Oxford Road, Manchester, UK M13 9PL*

† Electronic supplementary information (ESI) available: Table SI1: C–O, N–C and C–C bond lengths in the structures of: ^{Bz}LH·0.5H_2O and ^{PhOMe}LH. Fig. SI1: Schematic representation of the intermolecular H-bonds in ^{Bz}LH·0.5H_2O. Table SI2: C–O, N–C and C–C bond lengths in **1**·4MeCN, **2**·2MeOH, **3**·2MeCN and **4**·2MeCN. Fig. SI2: (a) Schematic representation of the intramolecular π–π interactions between the two ligands L and L^{A} of **2** in **2**·2MeOH. For clarity, only the rings involved in these interactions are shown. (b) A representation of the parameters involved in the interactions Ph/PhO and Ph/IM in **2**. Table SI3: Geometrical parameters for the π–π stacking interactions in **2** in **2**·2MeOH. Fig. SI3: X-Band EPR spectra of **1** and **2** at 77 K. Table SI4: Spin-Hamiltonian parameters for the compounds **1** and **2** obtained by simulation of the X-band frozen solution spectra. See DOI: 10.1039/b513221p

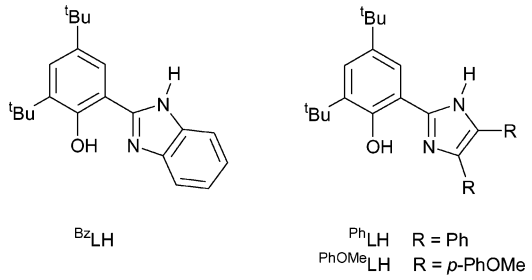

^{Bz}LH

^{Ph}LH R = Ph
^{PhOMe}LH R = *p*-PhOMe

$Cu^{R}L_2$: **1** (R = Bz), **2** (R = PhOMe)
$Zn^{R}L_2$: **3** (R = Bz), **4** (R = PhOMe)

Scheme 1

O–H group and an imidazole nitrogen atom.[11] ^{Ph}LH undergoes a reversible, one-electron, oxidation to produce $[^{Ph}LH]^{\bullet+}$, the W-band EPR spectrum of which is consistent with this species being comprised of a phenoxyl radical hydrogen-bonded to an imidazolium cation.[10] $[M(^{Ph}L)_2]$ (M = Cu or Zn) have been synthesised and shown to undergo two, reversible, one-electron, oxidations.[11] The first oxidation has been achieved chemically by reaction with $Ag[BF_4]$ (1 : 1) and $[M(^{Ph}L)_2][BF_4]$ have been isolated and structurally characterised. The bond lengths observed, when compared to those of the parent compound, together with the EPR and UV/vis spectroscopic properties of the cations, indicate that each involves an M(II) centre bound to a phenoxide ($^{Ph}L^-$) and a phenoxyl radical ($^{Ph}L^{\bullet}$) ligand. Also, we have reported the synthesis of the pro-ligands ^{Bz}LH and ^{PhOMe}LH (Scheme 1), the preparation and characterisation of $[Co(^{R}L)_2]$ (R = Ph, PhOMe or Bz) and $[Co(^{Bz}L)_3]$, and shown that oxidation of each of these compounds produces a phenoxyl radical complex.[15]

Herein we report the structural characterisation of the pro-ligands ^{Bz}LH and ^{PhOMe}LH, the electrochemical oxidation of each and the UV/vis spectrum of the product. These pro-ligands have been used to synthesise $[M(^{R}L)_2]$ (M = Cu or Zn; R = Bz or PhOMe) and each has been structurally characterised; the redox properties of these compounds have been investigated and the nature of the oxidation products probed by UV/vis and EPR spectroscopy. The results obtained are consistent with oxidation of both the pro-ligands and the complexes producing a phenoxyl radical that is stabilised, either by an intramolecular hydrogen bond or by coordination to a metal.

Experimental

$Cu(BF_4)_2{\cdot}H_2O$, $Zn(BF_4)_2{\cdot}H_2O$ and anhydrous MeOH were obtained from Aldrich Chemical Ltd.; CH_2Cl_2 and MeCN were freshly distilled under N_2 from CaH_2. The pro-ligands ^{Bz}LH and ^{PhOMe}LH were prepared as described previously;[15] diffusion of *n*-hexane into a $CHCl_3$ solution of the former and a CH_2Cl_2 solution of the latter, yielded single crystals of ^{Bz}LH·0.5H_2O and ^{PhOMe}LH, respectively, that were suitable for analysis by X-ray diffraction.

Syntheses of $[M(^{R}L)_2]$ (M = Cu or Zn; R = Bz or PhOMe)

General procedure. A solution containing two equivalents of the pro-ligand (^{R}LH; R = Bz or PhOMe) in the minimum volume of MeOH was added to a solution of $M(BF_4)_2{\cdot}H_2O$ (M = Cu or Zn) in MeOH (2–5 cm^3). The reaction mixture was stirred at room temperature for *ca.* 1 h, after which time an excess (a few drops) of Et_3N was added. After further stirring for *ca.* 1 h, each product was isolated and purified according to the procedure described below for each compound.

$[Cu(^{Bz}L)_2]$ (1). $Cu(BF_4)_2{\cdot}H_2O$ (317 mg, 1.24 mmol) in MeOH (5 cm^3) and ^{Bz}LH (800 mg, 2.48 mmol) in MeOH (50 cm^3) were used as described above. The solvent was removed *in vacuo* from the resultant brown solution and a dark brown solid was obtained. This material was dissolved in Et_2O, the mixture filtered, and the filtrate evaporated to dryness *in vacuo*; the brown solid obtained was dissolved in MeCN. This solution was filtered and the solvent allowed to evaporate by exposure to air; after 3–4 days, light brown, plate-like, single crystals of **1**·4MeCN were obtained. These were collected by filtration, crushed and dried *in vacuo*; the solid was dissolved in CH_2Cl_2, the solvent evaporated *in vacuo* and **1** obtained as a brown powder in 85% yield. Elemental analysis: Calc. for $C_{42}H_{50}N_4O_2Cu$: C 71.41, H 7.13, N 7.93. Found: C 70.91, H 7.50, N 7.76%. Positive FAB-MS: *m*/*z* 705 $\{M^+\}$. UV/vis (CH_2Cl_2): λ_{max}/nm (ε/M^{-1} cm^{-1}): 458 (460, sh), 657 (248).

$[Cu(^{PhOMe}L)_2]{\cdot}$2MeOH (2·2MeOH). $Cu(BF_4)_2{\cdot}H_2O$ (264 mg, 1.03 mmol) in MeOH (5 cm^3) and ^{PhOMe}LH (1 g, 2.07 mmol) in MeOH (200 cm^3) were used as described above. The resultant dark purple–brown solution was allowed to stand at room temperature exposed to air for 6 days; red–purple, block-like, single crystals of **2**·2MeOH were obtained. These crystals were collected by filtration, washed with MeOH, crushed and dried *in vacuo*, and **2**·2MeOH obtained as a dark purple–brown powder in 86% yield. Elemental analysis: Calc. for $C_{62}H_{70}N_4O_6Cu{\cdot}$2MeOH: C 70.22, H 7.13, N 5.12. Found: C 69.77, H 6.98, N 5.25%. Positive FAB-MS: *m*/*z* 1030 $\{M^+\}$. UV/vis (CH_2Cl_2): λ_{max}/nm (ε/M^{-1} cm^{-1}): 508 (769), 694 (553).

$[Zn(^{Bz}L)_2]{\cdot}$2MeOH (3·2MeOH). $Zn(BF_4)_2{\cdot}H_2O$ (240 mg, 0.93 mmol) in MeOH (5 cm^3) and ^{Bz}LH (600 mg, 1.86 mmol) in MeOH (200 cm^3) were reacted as described above. A white precipitate formed upon mixing and the reaction mixture was left to stand at −30 °C for *ca.* 48 h to ensure completion of the reaction. The precipitate was collected by filtration, washed with cold MeOH, dried *in vacuo* and **3**·2MeOH obtained as a white powder in 82% yield. A solution of **3** in MeCN at room temperature exposed to the air afforded, after 2–4 days, colourless, block-like, single crystals of **3**·2MeCN. Elemental analysis: Calc. for $C_{42}H_{50}N_4O_2Zn{\cdot}$2MeOH: C 68.42, H 7.57, N 7.25. Found: C 68.00, H 7.06, N 7.41%. Positive FAB-MS: *m*/*z* 707 $\{M^+\}$.

$[Zn(^{PhOMe}L)_2]{\cdot}$2MeOH (4·2MeOH). $Zn(BF_4)_2{\cdot}H_2O$ (266 mg, 1.03 mmol) in MeOH (5 cm^3) and ^{PhOMe}LH (1 g, 2.07 mmol) in MeOH (200 cm^3) were used as described above. The resultant colourless solution was exposed to air and allowed to evaporate at room temperature for some 6 days and a white crystalline powder was obtained. The powder was collected by filtration, washed with MeOH, crushed, dried *in vacuo*, and **4**·2MeOH obtained as a white powder in 85% yield. The product was found to be light sensitive and, therefore, was stored in absence of light. Evaporation of a solution of **4** in CH_2Cl_2–MeCN (1 : 1) at room temperature, after 2–4 days exposure to air, afforded colourless, triangular-prism-like, single crystals of **4**·2MeCN. Elemental analysis: Calc. for $C_{62}H_{70}N_4O_6Zn{\cdot}$2MeOH: C 70.11, H 7.12, N 5.43. Found: C 70.23, H 7.05, N 5.29%. Positive FAB-MS: *m*/*z* 1031 $\{M^+\}$.

Synthesis of $[M(^{PhOMe}L_2)][BF_4]$ (M = Cu or Zn)

General procedure. Each reaction was carried out in a pre-dried Schlenk vessel in the absence of light under an Ar atmosphere, and using a freshly distilled solvent. A solution of $[M(^{R}L)_2]$ (M = Cu or Zn; R = Bz or PhOMe) in CH_2Cl_2 was added to a suspension of $Ag[BF_4]$ (1 eq.) in CH_2Cl_2 at −10 °C (ice/acetone bath). The colour of the solution darkened rapidly and a silver mirror formed. The mixture was stirred for *ca.* 1 h at −10 °C, warmed to room temperature, stirred for *ca.* 30 min, then filtered through glass wool mounted at one end of a Teflon cannula (in some instances, the use of a metal cannula induced a colour change of the solution and, therefore, such contact was avoided). The solvent was evaporated from the filtrate under a reduced pressure; [**2**][BF_4] and [**4**][BF_4] were each isolated as a dark green solid; however, it proved difficult to isolate solid samples of [**1**][A] and [**3**][A] ([A] = $[BF_4]^-$ or $[PF_6]^-$).

[2][BF_4]. A solution of **2** (166 mg, 0.161 mmol) in CH_2Cl_2 (20 cm^3) and a suspension $Ag[BF_4]$ (31.5 mg, 0.161 mmol) in CH_2Cl_2 (5 cm^3) were reacted and the product isolated as described above. The resultant dark green solid was washed with CH_2Cl_2–*n*-hexane 1 : 3 (2 × 10 cm^3), to remove any unreacted **2**, and then dried *in vacuo*. The solid obtained was recrystallised by the diffusion of *n*-hexane into a CH_2Cl_2 solution at 4 °C under an Ar atmosphere. After a few days, [**2**][BF_4]·$2CH_2Cl_2$ (~140 mg; 85% yield) was obtained as a fluffy green material. Elemental analysis: Calc. for $C_{62}H_{70}N_4O_6CuBF_4 \cdot 2CH_2Cl_2$: C 59.60, H 5.74, N 4.34. Found: C 59.50, H 5.69, N 4.45%. Positive FAB-MS: *m*/*z* 1031 $\{(M + 1)^+\}$.

[4][BF_4]. A solution of **4** (94 mg, 0.088 mmol) in CH_2Cl_2 (15 cm^3) and a suspension of $Ag[BF_4]$ (17.3 mg, 0.088 mmol) in CH_2Cl_2 (5 cm^3) were reacted and the product isolated as described above. The resultant dark green solid was dried *in vacuo* and recrystallised by diffusion of *n*-hexane into a CH_2Cl_2 solution at 4 °C under an Ar atmosphere. After *ca.* 4 days, [**4**][BF_4] was obtained as dark green, microcrystalline, needles (~75 mg; 70% yield). Elemental analysis: Calc. for $C_{62}H_{70}N_4O_6ZnBF_4$: C 66.52, H 6.26, N 5.01. Found: C 66.77, H 6.38, N 5.07%. Positive FAB-MS: *m*/*z* 1032 $\{(M + 1)^+\}$.

Physical methods

Elemental analyses of the compounds isolated in these studies were accomplished in the Microanalytical Laboratory of the School of Chemistry; University of Nottingham. FAB and EI mass spectra were recorded on a Fisons VG Trio 200 or a Fisons VG Autospec spectrometer. 300 MHz ^{1}H-spectra were recorded on a Bruker DPX300 NMR spectrometer, EPR spectra were recorded on a Bruker X-band EMX spectrometer, and UV/vis spectra were recorded on a Perkin Elmer Lambda 5 spectrophotometer.

The cyclic voltammogram (CV) of each compound, in CH_2Cl_2 (1 mM) at room temperature, containing $[NBu^n_4][BF_4]$ (0.4 M) as the background electrolyte, was recorded using a glassy carbon working electrode, a Pt wire secondary electrode, and a saturated calomel reference electrode (SCE). Thus, potentials were measured *vs*. SCE, but are quoted *vs.* the $[(\eta^5\text{-}C_5H_5)_2Fe]^+/[(\eta^5\text{-}C_5H_5)_2Fe]$ ($[Fc]^+/[Fc]$) couple used as an internal standard. When necessary, to avoid overlapping redox couples, the $[(\eta^5\text{-}C_5Me_5)_2Fe]^+/[(\eta^5\text{-}C_5Me_5)_2Fe]$ couple was used as the internal reference and the potentials of redox process(es) observed referenced to the $[Fc]^+/[Fc]$ couple by an independent calibration ($\Delta E_{1/2}$, $[Fc]^+/[Fc] - [(\eta^5\text{-}C_5Me_5)_2Fe]^+/[(\eta^5\text{-}C_5Me_5)_2Fe] = 0.526$ V). Coulometric measurements were performed at room temperature for the compound of interest dissolved in CH_2Cl_2 containing $[NBu^n_4][BF_4]$ (0.4 M); the cell consisted of a Pt/Rh gauze basket working electrode, a Pt/Rh gauze secondary electrode, and a saturated calomel reference electrode. CV and controlled potential electrolysis measurements were performed using an Autolab PGSTAT20 potentiostat.

UV/vis spectroelectrochemistry was accomplished for the compound of interest dissolved in CH_2Cl_2 containing $[NBu^n_4][BF_4]$ (0.4 M) in an optically transparent electrochemical (OTE) cell (modified quartz cuvette, optical pathlength: 0.5 mm). A three-electrode configuration was used in the cell, comprising a Pt/Rh gauze working electrode, a Pt wire secondary electrode contained in a fritted PTFE sleeve, and a saturated calomel electrode isolated from the test solution by a bridge tube containing the electrolyte solution retained by a porous frit. The potential at the working electrode was controlled by a Sycopel Scientific Ltd. DD10M potentiostat. UV/vis spectra were recorded on a Perkin Elmer Lambda 16 spectrophotometer; during the measurements the spectrometer cavity was purged with N_2 and temperature control at the sample was achieved by flowing cooled N_2 across the surface of the cell.

The unit cell, data collection, and refinement parameters for ^{Bz}LH·0.5H_2O, ^{PhOMe}LH, **1**·4MeCN, **2**·2MeOH, **3**·2MeCN and **4**·2MeCN are given in Table 1. Diffraction data for ^{Bz}LH·0.5H_2O, **3**·2MeCN and **4**·2MeCN were collected on a Bruker SMART 1000 CCD area detector diffractometer; those of ^{PhOMe}LH were collected using a Stadi-4 circle diffractometer using ω-scans. For **1**·4MeCN and **2**·2MeOH, diffraction data were collected on a Nonius kappa CCD using ω and ϕ scans. Each instrument was equipped with an Oxford Cryosystem open-flow nitrogen cryostat[16] and graphite-monochromated Mo-Kα radiation (0.71073 Å) was used in all cases. Data were corrected for Lorentz and polarisation effects. We thank the EPSRC National Crystallographic Service at Southampton University for collecting the data for **1**·4MeCN and **2**·2MeOH.The structures of ^{Bz}LH·0.5H_2O, ^{PhOMe}LH, **1**·4MeCN, **2**·2MeOH and **3**·2MeCN were each solved by direct methods and that of **4**·2MeCN by Patterson methods using SHELXS 97.[17] All structures were refined against F^2 using SHELXL 97.[17] Unless otherwise stated, all non-H atoms were refined with anisotropic atomic displacement parameters (adps). The hydrogen atoms of OH_{phenol} (for each pro-ligand), OH_{water}, CH_3CN and CH_3OH were located by difference Fourier syntheses and their positions refined as part of a rigid rotor, except for the OH_{water} which were freely refined. All other H-atoms were placed in geometrically calculated positions and refined as part of a riding model, with $U(H)_{iso} = 1.2U_{eq}(C)$ or (N) for C and N aromatic hydrogen atoms and $U(H)_{iso} = 1.5U_{eq}(C)$, for C$H_3$. For **1**·4MeCN, geometrical restraints were applied to each MeCN molecule. For **2**·2MeOH, the hydrogen of one OH_{MeOH} group could not be located. Disorder was present in the PhOMe groups and all the phenyl ring atoms, except C6 and C11, were modelled over two half occupied sites with isotropic adps and restraints.

The ^{t}Bu group defined by C30 also showed disorder and C32 and C33 were modelled over two partially occupied sites with occupancies 0.65 and 0.35. For **4**·2MeCN, one OMe group showed

Table 1 Crystallographic data for ^{Bz}LH·0.5H$_2$O, ^{PhOMe}LH, **1**·4MeCN, **2**·2MeOH, **3**·2MeCN and **4**·2MeCN

	^{Bz}LH·0.5H$_2$O	^{PhOMe}LH	**1**·4MeCN	**2**·2MeOH	**3**·2MeCN	**4**·2MeCN
Empirical formula	$C_{21}H_{27}N_2O_{1.5}$	$C_{31}H_{36}N_2O_3$	$CuC_{50}H_{62}N_8O_2$	$CuC_{64}H_{78}N_4O_8$	$ZnC_{46}H_{56}N_6O_2$	$ZnC_{66}H_{76}N_6O_6$
M_r	331.45	484.62	870.62	1094.84	790.34	1114.70
Crystal system	Monoclinic	Monoclinic	Triclinic	Triclinic	Monoclinic	Triclinic
Space group	$P2_1/n$	$P2_1/n$	$P\bar{1}$	$P\bar{1}$	$C2/c$	$P\bar{1}$
a/Å	12.245(2)	13.954(8)	10.0084(3)	12.9669(8)	26.595(4)	11.273(1)
b/Å	16.869(3)	14.412(9)	13.0262(4)	13.2272(8)	8.1200(1)	12.359(2)
c/Å	19.161(4)	14.086(12)	20.3503(8)	18.4793(11)	20.435(3)	22.334(3)
α/°	90	90	94.968(2)	102.802(3)	90	89.689(2)
β/°	104.79(3)	102.38(7)	93.835(2)	98.699(3)	103.777(2)	85.560(2)
γ/°	90	90	112.255(3)	108.413(3)	90	79.024(2)
V/Å^3	3826.7(13)	2767(3)	2431.9(2)	2847.4(3)	4286.0(1)	3045.4(7)
Z	8	4	2	2	4	2
T/K	150	150	120	120	150	150
D_c/g cm^{-3}	1.151	1.163	1.189	1.256	1.225	1.216
μ(Mo-Kα)/mm^{-1}	0.072	0.075	0.495	0.443	0.617	0.458
Reflections collected	23946	6076	39596	43424	11464	30267
Independent reflections (R_{int})	8886 (0.0511)	5477(0.3326)	9891 (0.1047)	17368 (0.126)	5081 (0.039)	14062 (0.028)
Observed reflections [$I > 2\sigma(I)$]	4326	2999	5967	3891	3419	10632
R	0.0407	0.112	0.0636	0.0677	0.0374	0.0438
R_w	0.1170	0.299	0.1762	0.1726	0.0845	0.1268

disorder and was refined over two sites with occupancies of 0.7 : 0.3; geometrical restraints were applied and the C and O atoms involved were refined with isotropic adps.

CCDC reference numbers 284612–284617

For crystallographic data in CIF or other electronic format see DOI: 10.1039/b513221p

Results and discussion

Structure of the pro-ligands ^{R}LH (R = Bz or PhOMe)

The pro-ligands ^{Bz}LH and ^{PhOMe}LH were synthesised as described previously[15] and the structures of ^{Bz}LH·0.5H$_2$O and ^{PhOMe}LH have been determined by X-ray crystallography. The molecular structure (Fig. 1) and the dimensions (Tables SI1a and SI1b, ESI†) of ^{Bz}LH and ^{PhOMe}LH are each consistent with the corresponding aspects of ^{Ph}LH[11] and other, related, organic species.[18] Each pro-ligand possesses an intramolecular O–H···N hydrogen-bond involving the phenolic O–H group and an imidazole nitrogen, as indicated by the O(1)···N(5) distance (2.54–2.61 Å) and the O(1)–H(1)···N(5) interbond angle (141–151°) (Table 2). These values are similar to those for the hydrogen bonds of: ^{Ph}LH·Me$_2$CO (O···N 2.596(2) Å, O–H···N 150.7°);[11] 2-(2′-hydroxyphenyl)imidazole (ImPhOH) (O···N 2.545(2) Å, O–H···N 154(3)°);[19] 2-(pyrazol-1′-yl)- and 2,5-bis(pyrazol-1′-yl)-1,4-dihydroxybenzene (O···N 2.558(9) and 2.612(3) Å; O–H···N 138(9) and 149(4)°, respectively);[20] and 2-(2-hydroxyphenyl)pyrimidine (O···N 2.511(3) Å; O–H···N 153(5)°).[21] In ^{Ph}LH·Me$_2$CO[11] and ^{PhOMe}LH the imidazole and phenol rings are approximately coplanar, with the angle between the planes of these rings being 7.7 and 2.6°, respectively. The asymmetric unit of ^{Bz}LH·0.5H$_2$O contains two molecules (connected by hydrogen bonding *via* a H$_2$O molecule; Fig. SI1, ESI†). The angle between the planes of the phenol and imidazole rings in one molecule (I) is 6.9 and 17.0° in the other (II) and the O(H)···N distances are 2.539(2) and 2.609(2) Å, respectively (Table 2). The greater twist in II appears to arise due to an O1A···H1S–O1S hydrogen-bond involving the water molecule defined by atom O1S that is *ca.* perpendicular to the plane of the phenol ring; this interaction leads to the C–O1A bond in (II) (1.378(2) Å) being longer than that in (I) (1.366(2) Å).

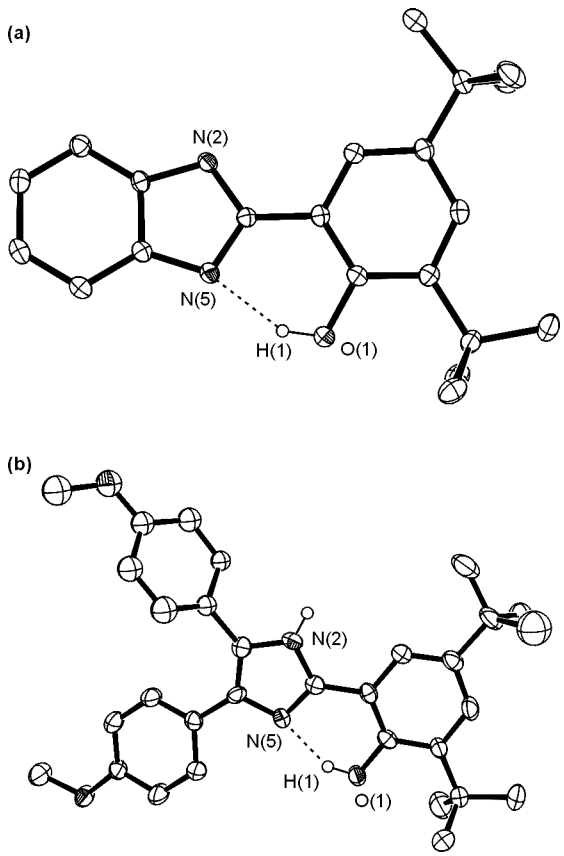

Fig. 1 ORTEP representation of the structure of ^{R}LH (R = Bz or PhOMe) in (a) ^{Bz}LH·0.5H$_2$O and (b) ^{PhOMe}LH.

The 300 MHz ^{1}H NMR spectrum of each ^{R}LH (R = Ph, Bz or PhOMe) pro-ligand in CDCl$_3$ at 298 K is independent

Table 2 Geometrical parameters for the intramolecular H-bonds of ^{Bz}LH·0.5H$_2$O and ^{PhOMe}LH

		O–H[a]/Å	H···N/Å	O···N/Å	OH···N/°	Phenol/Im twist angle/°
^{Bz}LH·0.5H$_2$O[b]	I	0.84	1.77	2.539(2)	150.7	6.9
	II	0.84	1.85	2.609(2)	140.7	17.0
^{PhOMe}LH		0.84	1.84	2.605(6)	150.4	2.6

[a] The length of the O–H bond has been restrained to 0.84 Å for each structure described. [b] Two molecules of ^{Bz}LH are present in the asymmetric unit.

of concentration (dilution factors: 10^{-1} and 10^{-2}). The $^1HO_{phenol}$ resonance was observed at *ca.* 13.3 ppm (13.1, ^{Ph}LH; 13.6, ^{Bz}LH; and 13.2, ^{PhOMe}LH) and this is consistent[22] with each pro-ligand in $CDCl_3$ solution retaining the intramolecular O–H···N hydrogen bond identified in the solid state. The $^1HO_{phenol}$ resonance at *ca.* 13 ppm was distinguished from that of the imidazole NH group (at *ca.* 9 ppm) by comparison with the ^{1}H NMR spectrum of the *N*-methyl substituted analogue of ^{Ph}LH which exhibits only a $^1HO_{phenol}$ resonance.

Electrochemical oxidation of ^{R}LH: formation of [^{R}LH]$^{\bullet+}$ (R = Bz or PhOMe)

The cyclic voltammogram (CV) of each ^{R}LH (R = Bz or PhOMe), in CH_2Cl_2, at 298 K containing [NBu_4^n][BF_4] (0.4 M) (Fig. 2), is analogous to that of ^{Ph}LH.[11] Thus, each CV exhibits a one-electron oxidation process that is reversible over the range of scan rates investigated (20–500 mV s^{-1}). The nature of the oxidation observed for ^{R}LH (R = Ph,[11] Bz or PhOMe) is in marked contrast to the irreversible, two-electron, oxidation generally observed for a phenol.[23] For example, electrochemical oxidation of 2,4,6-tri-*tert*-butylphenol (^{t}Bu$_3$PhOH)[24] proceeds as:[25] (i) a one-electron oxidation to form [^{t}Bu$_3$PhOH]$^{\bullet+}$; (ii) deprotonation of this cation (pK_a *ca.* −5)[23] to form [^{t}Bu$_3$PhO]$^{\bullet}$; (iii) this radical is easier to oxidise than the parent phenol[26] and undergoes a one-electron oxidation to produce the phenoxonium ion, [^{t}Bu$_3$PhO]$^+$.

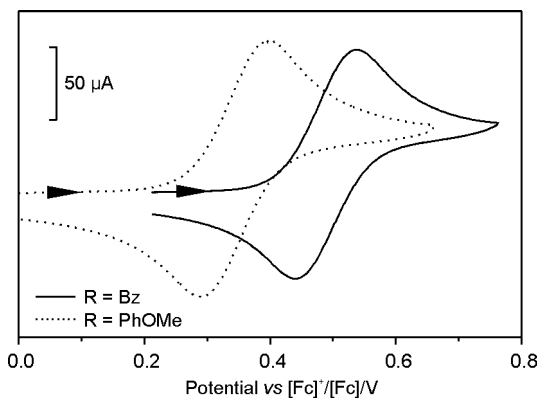

Fig. 2 Cyclic voltammograms of ^{R}LH (R = Bz, —; PhOMe, ···) recorded at a scan rate of 100 mV s^{-1} using a glassy carbon working electrode for a *ca.* 1 mM solution in CH_2Cl_2 at 298 K containing [NBu_4^n][BF_4] (0.4 M) as the supporting electrolyte. The potential is expressed relative to the [Fc]$^+$/[Fc] couple recorded under the same conditions.

Spectroelectrochemical experiments have been performed in order to investigate the nature of [^{R}LH]$^{\bullet+}$ (R = Bz or PhOMe), each of which is stable for *ca.* 1 h in CH_2Cl_2 under N_2 at 273 K. The one-electron oxidation of each ^{R}LH leads to a significant colour change; from colourless to dark blue (R = PhOMe) or bright yellow–green (R = Bz). The UV/vis spectrum of both [^{PhOMe}LH]$^{\bullet+}$ and [^{Bz}LH]$^{\bullet+}$ (Fig. 3 and Table 4), like that of [^{Ph}LH]$^{\bullet+}$ (Table 4),[11] possesses a band with λ_{max} *ca.* 400 nm (ε 5–10000 M^{-1} cm^{-1}) that is typical of $\pi \rightarrow \pi^*$ transition of a phenoxyl radical.[7,8,23] Also, each [^{R}LH]$^{\bullet+}$ exhibits a broad absorption at *ca.* 740 nm with an intensity (ε 1600, 5600 or 13500 M^{-1} cm^{-1}) that varies with the nature of R (Table 4).

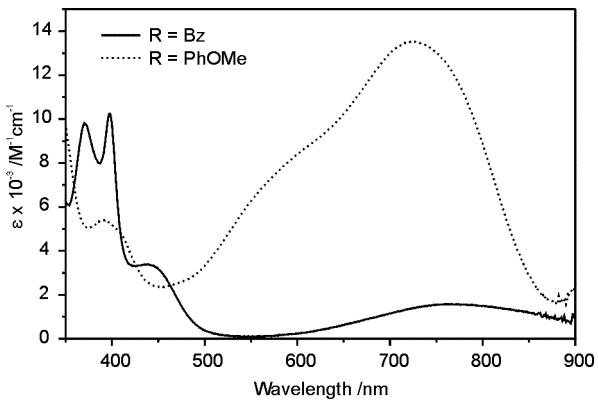

Fig. 3 UV/vis spectra of [^{R}LH]$^{\bullet+}$ (R = Bz, —; PhOMe, ···) electrochemically generated from ^{R}LH (*ca.* 1 mM) in CH_2Cl_2 containing [NBu_4^n][BF_4] (0.4 M) in an OTE cell at 273 K.

The X-band EPR spectrum of each [^{R}LH]$^{\bullet+}$ (R = Ph,[11] Bz or PhOMe) in CH_2Cl_2 solution at 77 K comprises a single isotropic signal with g_{iso} 2.004–2.005, a line width of *ca.* 10 G and no resolved hyperfine splitting or anisotropy. The relatively narrow line width indicates that any hyperfine splitting is small, suggesting that the unpaired electron is not localised to any appreciable extent on the imidazole nitrogen atoms. The W-band EPR spectrum of each [^{R}LH]$^{\bullet+}$ (R = Ph, Bz or PhOMe) has been interpreted using density functional theoretical (DFT) calculations.[10] The results obtained indicate that each [^{R}LH]$^{\bullet+}$ should be regarded as a phenoxyl radical since the majority of the spin density is localised on the phenoxyl ring: 90% [^{Bz}LH]$^{\bullet+}$; 80% [^{Ph}LH]$^{\bullet+}$; 65% [^{PhOMe}LH]$^{\bullet+}$. An important result obtained from these studies[10] is that each [^{R}LH]$^{\bullet+}$ (R = Ph, Bz or PhOMe) involves an intramolecular O···H–N hydrogen bond between the phenoxyl radical and the imidazolium group. Thus, Scheme 2, oxidation of ^{R}LH to [^{R}LH]$^{\bullet+}$ proceeds *via* proton-coupled electron transfer (PCET), *i.e.* the e$^-$ and H$^+$ are transferred in one kinetic step with no intermediate on the reaction coordinate.[8,9] The presence of the O–H···N hydrogen-bond in the parent molecule, the strong acidity of a phenoxyl radical cation (p$K_a \ll 0$)[23] and the basic nature of an imidazole nitrogen (pK_b *ca.* 7) combine to facilitate the PCET. This mechanism is analogous to that proposed for the electrochemically reversible, one-electron,

Table 3 Cyclic voltammetric data[a] for ^{Bz}LH, ^{PhOMe}LH and **1–4**

Complex	$[LH]^{\bullet+}/[LH]$ $E_{1/2}$/V (ΔE/mV)	$[M(L^{\bullet})(L)]^{+}/[M(L)_2]$ $E_{1/2}$/V (ΔE/mV)	$[M(L^{\bullet})_2]^{2+}/[M(L^{\bullet})(L)]^{+}$ $E_{1/2}$/V (ΔE/mV)	$\Delta E([Fc]^{+}/[Fc])$/mV
^{Bz}LH	0.49 (100)			110
^{PhOMe}LH	0.34 (100)			100
1[b]		0.36 (70)	0.58 (110)	90
2[c]		0.11 (70)	0.44 (90)	120[d]
3		0.41[e]	0.58[e]	
4		0.18 (80)	0.47 (130)	90[d]

[a] Recorded in CH_2Cl_2 containing $[NBu^n_4][BF_4]$ (0.4 M) as the supporting electrolyte at a scan rate of 100 mV s^{-1}, unless stated otherwise; potentials in V *vs.* $[Fc]^{+}/[Fc]$, at 298 K. [b] A reduction at $E_p^c = -1.82$ V is tentatively assigned to a Cu^{II}/Cu^{I} couple. [c] A reduction at $E_p^c = -1.81$ V is tentatively assigned to a Cu^{II}/Cu^{I} couple. [d] The $[(\eta^5\text{-}C_5Me_5)_2Fe]^{+}/[(\eta^5\text{-}C_5Me_5)_2Fe]$ couple was used as the internal standard. [e] Determined by square wave voltammetry.

Table 4 Absorptions observed in the UV/vis spectrum of the product of the one-electron oxidation of ^{R}LH (R = Bz or PhOMe) (at 273 K) and **1–4** (at 298 K) in an OTE cell for a solution of compound (*ca.* 1 mM) in CH_2Cl_2 containing $[NBu^n_4][BF_4]$ (0.4 M)

Species	λ_{max}/nm (ε/M^{-1} cm^{-1})	Isosbestic points/nm
$[^{Bz}LH]^{\bullet+}$	370 (9700); 397 (10200); 434br (3400); 764 (1600)	348
$[^{PhOMe}LH]^{\bullet+}$	388 (5400); 408sh (4800); 560br sh (6700); 726 (13500)	355
$[^{Ph}LH]^{\bullet+}$ [11]	379 (9700), 401 (9200), 514 (4000), 715(5600)	351
1	370 (15400); 458sh (450); 657 (250)	
[**1**]$^{+}$	360br (13500); 415–435sh (2300–1600); 506 (2300); *ca.* 900	357, 400
2	367 (32300); 508 (750); 694 (550)	
[**2**]$^{+}$	372 (21500); 410 (11300); 582 (6200)	347, 391
3	372 (28900)	
[**3**]$^{+}$	371 (24800); 508 (3200); *ca.* 900	341, 393
4	291 (36400); 359 (37500)	
[**4**]$^{+}$[a]	409sh (5600); 542sh (8100); 580 (10800); 698br (8700); 792sh (5900)	341, 390

[a] The extinction coefficients were calculated for the last spectrum for which a tight isosbestic point was observed.

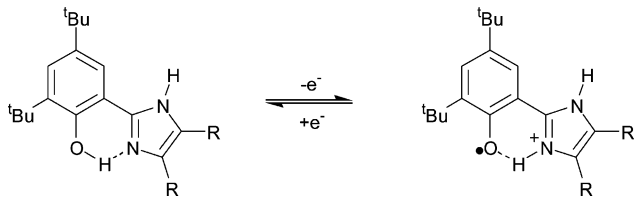

Scheme 2

oxidation of an α-alkylaminophenol to form a hydrogen-bonded phenoxyl/ammonium radical cation.[7–9]

The potentials for the oxidation of ^{R}LH to $[^{R}LH]^{\bullet+}$: $E_{1/2}$/V = 0.49 (R = Bz), 0.43 (R = Ph),[11] or 0.34 (R = PhOMe) (*vs.* $[Fc]^{+}/[Fc]$) are each significantly lower than that for the oxidation of 2,4,6-tri-*tert*-butylphenol (1.20 V *vs.* $[Fc]^{+}/[Fc]$),[8,24] but are comparable with those reported for the oxidation of α-alkylaminophenols possessing an intramolecular H-bond,[7,8] Thus, the potential of a phenoxyl/phenol couple is lowered by the involvement of the phenoxyl radical in a hydrogen bond; an observation relevant to the potential at which a Tyr$^{\bullet}$/Tyr redox couple operates in proteins.[1–4]

[M(^{R}L)$_2$] complexes (M = Cu or Zn; R = Bz or PhOMe)

Synthesis and structural characterisation. The reaction of $M(BF_4)_2{\cdot}H_2O$ (M = Cu or Zn) with ^{R}LH (R = Bz or PhOMe) (1 : 2) in the presence of an excess of Et_3N yields the corresponding $[M(^{R}L)_2]$ compound: $[Cu(^{Bz}L)_2]$ (**1**), $[Cu(^{PhOMe}L)_2]$ (**2**), $[Zn(^{Bz}L)_2]$ (**3**) and $[Zn(^{PhOMe}L)_2]$ (**4**). Each compound has been isolated, crystallised, and the structures of **1**·4MeCN, **2**·2MeOH, **3**·2MeCN and **4**·2MeCN have been determined using X-ray crystallography (Table 1, Fig. 4)). In each compound, each imidazole N–H group forms a hydrogen bond to an atom of an adjacent solvent molecule possessing a lone pair of electrons (*i.e.* MeC*N* or Me*O*H); also, for **2**·2MeOH, there is a hydrogen bond between the Me*OH* group and the $O_{phenolate}$ of a ligand (Fig. 4(b)).

In each compound, each ligand acts as an *N*,*O*-bidentate chelate and the metal centre possesses an N_2O_2-coordination sphere (Fig. 4). The lengths of the M–O and M–N bonds (Table 5) are similar to those of the corresponding bonds of bis(salicylaldiminato)M(II) complexes,[27] implying that each complex is comprised of a M(II) centre bound to two phenolate ligands. This is supported by the C–O bond lengths (1.318(2)–1.331(2) Å, Table SI2, ESI†) that are typical of a phenolate[18] and significantly longer than the C–O bond length of ^{Ph}L$^{\bullet}$ (1.264(5) Å) in $[Cu(II)(^{Ph}L)(^{Ph}L^{\bullet})][BF_4]$.[11] There are some small perturbations in the length of the M–O and M–N bonds in **1**·4MeCN and **2**·2MeOH due to hydrogen bonding interactions with the co-crystallised solvent molecules; *e.g.* in **2**·2MeOH, O(1A), but not O(1), forms a hydrogen bond to MeOH (Fig. 4) and Cu–O(1A) (1.917(4) Å) is slightly, but significantly, longer than Cu–O(1) (1.890(4) Å).

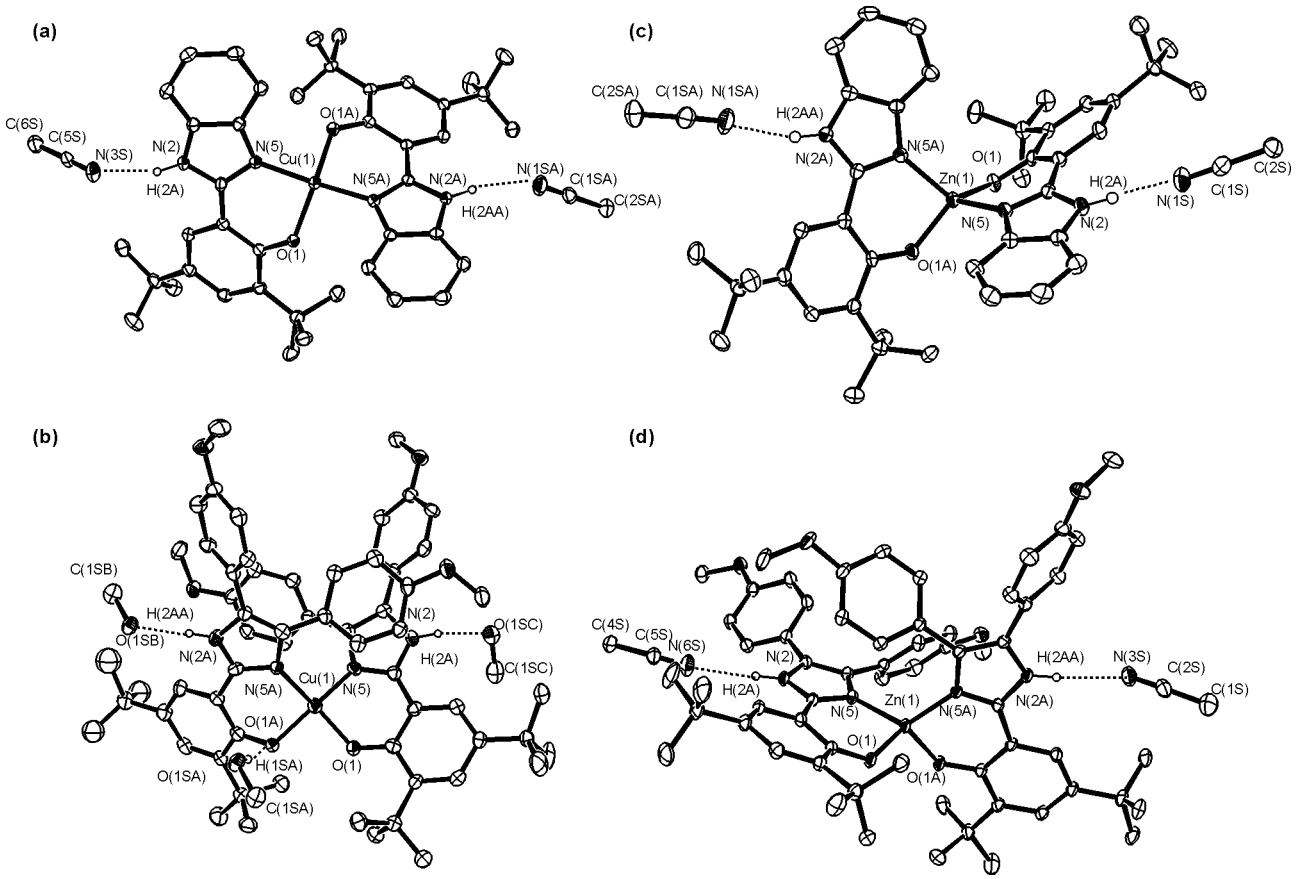

Fig. 4 ORTEP representations of the molecular structure of $[M(^{R}L)_2]$ (plus hydrogen-bonded solvent molecules) in: (a) $[Cu(^{Bz}L)_2]$ in **1**·4MeCN, (b) $[Cu(^{PhOMe}L)_2]$ in **2**·2MeOH, (c) $[Zn(^{Bz}L)_2]$ in **3**·2MeCN and (d) $[Zn(^{PhOMe}L)_2]$ in **4**·2MeCN. Length of hydrogen bond/Å: N_{im}—H $\cdots$ N_{MeCN}: **1**·4MeCN H(2A) $\cdots$ N(3S) 2.124 and H(2AA) $\cdots$ N(1SA) 2.110; **3**·2MeCN H(2A) $\cdots$ N(1S) 2.126 and H(2AA) $\cdots$ N(1SA) 2.055; **4**·2MeCN H(2A) $\cdots$ N(6S) 2.055 and H(2AA) $\cdots$ N(3S) 2.055: **2**·2MeOH $_{MeOH}$O–H $\cdots$ N_{im}: H(2A) $\cdots$ O(1SC) 2.180 and H(2AA) $\cdots$ O(1SB) 1.921; $_{MeOH}$O–H $\cdots$ O_{PhO}/Å: O(1A) $\cdots$ O(1SA) 1.886.

Table 5 Selected bond lengths (Å) and angles (°) for **1**·4MeCN and **2**·2MeOH (M = Cu), **3**·2MeCN and **4**·2MeCN (M = Zn)

	1·4MeCN	**2**·2MeOH	**3**·2MeCN	**4**·2MeCN
M(1)–O(1A)	1.898(2)	1.917(4)	1.919(2)	1.911(2)
M(1)–O(1)	1.919(2)	1.890(4)	1.919(2)	1.929(2)
M(1)–N(5A)	1.933(3)	1.973(4)	1.979(2)	1.993(2)
M(1)–N(5)	1.947(3)	1.946(5)	1.979(2)	1.993(2)
O(1A)–M(1)–O(1)	155.46(11)	89.4(2)	117.88(8)	110.41(6)
N(5A)–M(1)–N(5)	160.66(12)	101.2(2)	121.85(9)	122.35(6)
O(1A)–M(1)–N(5)	92.54(11)	156.3(2)	115.66(6)	121.38(6)
O(1)–M(1)–N(5A)	93.97(11)	155.1(2)	115.66(6)	117.80(6)
O(1A)–M(1)–N(5A)	91.86(11)	89.1(2)	93.92(6)	94.42(6)
O(1)–M(1)–N(5)	89.8(1)	89.8(2)	93.92(6)	91.94(6)

The CuN_2O_2 centres of **1**·4MeCN and **2**·2MeOH each possesses a distorted square planar geometry; the angle between the CuN(5)O(1) and CuN(5A)O(1A) planes is 31.2° (**1**·4MeCN) and 33.6° (**2**·2MeOH); the N(5)–Cu–O(1) and N(5A)–Cu–O(1A) bond angles are 89.8(1), 91.86(11)° and 89.8(2), 89.1(2)° for **1**·4MeCN and **2**·2MeOH, respectively (Table 5). The ZnN_2O_2 centres of **3**·2MeCN and **4**·2MeCN are each distorted tetrahedral; the angle between the ZnN(5)O(1) and ZnN(5A)O(1A) planes is 86.6° (**3**·2MeCN) and 86.8° (**4**·2MeCN). The N(5)–Zn–O(1) and N(5A)–Zn–O(1A) bond angles are 93.92(6), 93.92(6)° and 91.94(6), 94.42(6)° for **3**·2MeCN and **4**·2MeCN, respectively (Table 5). Thus, in each $[M(^{R}L)_2]$ (M = Cu, Zn or Co[15]; R = Ph,[11] Bz or PhOMe) complex, the orientation of the two ligands accommodates the normal geometrical preference of the metal centre.

Intramolecular π–π interactions between the ligands L and L(A) are present in **2**·2MeOH (Fig. SI2 and Table SI3, ESI†). Each of these interactions involves the C(12)–C(17) or C(12A)–C(17A) phenyl ring of one ligand with: (i) the phenolate ring (PhO) of the second ligand; (ii) the imidazole ring of the second ligand; and/or (iii) the whole phenol/imidazole unit of the second ligand. The presence of analogous π–π interactions has been used to rationalise the *cis*-CuN_2O_2 geometries of $[Cu(^{Ph}L)_2]$·4DMF and $[Cu(^{Ph}L)_2]$·3MeOH[11] and it appears that the presence of 4,5-diarylimidazole groups in **2** also favours a *cis*-CuN_2O_2 geometry. In contrast, **1**, which cannot establish corresponding π–π interactions, possesses the *trans*-CuN_2O_2 coordination sphere.

UV/vis and EPR studies. The UV/vis spectra of **1** and **2** in CH_2Cl_2 (Table 4) are similar and each resembles that

of $[Cu(^{Ph}L)_2]$ in CH_2Cl_2.[11] Within the visible region, **1** and **2** manifest absorptions with λ_{max} of 458 (ε = 450 M^{-1} cm^{-1}) and 657 nm (ε = 250 M^{-1} cm^{-1}) and 508 (ε = 750 M^{-1} cm^{-1}) and 694 nm (ε = 550 M^{-1} cm^{-1}), respectively. In each case, the higher energy transition is assigned to a phenolate-to-Cu(II) charge transfer transition, on the basis of comparisons with the UV/vis spectra of other Cu(II)–phenolate complexes;[28,29] the lower energy feature is assigned to ligand-field transitions, *cf.* those of bis(salicylaldimino)Cu(II) complexes that also possess a distorted square planar geometry.[30] As expected for complexes involving a d^{10} metal centre, $[Zn(^{R}L)_2]$ (R = Ph,[11] Bz or PhOMe) do not display any absorption in the visible region.

The X-band EPR spectrum of both **1** and **2**, in CH_2Cl_2–DMF (9 : 1) solution at 77 K (Fig. SI3, ESI†), resembles that of $[Cu(^{Ph}L)_2]$[11] and is typical of a Cu(II) complex possessing a $(d_{x^2-y^2})^1$ ground state ($S = 1/2$) with $g_{zz} > g_{xx} \approx g_{yy} > g_e$.[31] Each spectrum shows hyperfine splitting in the g_{zz} region due to coupling of the unpaired electron to the $^{63,65}Cu$ ($I = 3/2$) nuclei; hyperfine and superhyperfine coupling to the $^{63,65}Cu$ and ^{14}N nuclei are manifest in the g_{xx} and g_{yy} regions. Spin-Hamiltonian parameters for the low-field features have been obtained using an in-house simulation program[32] (Table SI4, ESI†). The g_{zz} and A_{zz} values for **1** (2.254, 165 G), **2** (2.254, 164 G) and $[Cu(^{Ph}L)_2]$[11] (2.253, 164 G) are as expected for a tetragonal $\{Cu^{II}N_2O_2\}$ centre.[33] This information is consistent with both **1** and **2** in CH_2Cl_2–DMF (9 : 1) solution retaining the structure identified by X-ray crystallography.

Redox properties. The cyclic voltammograms of **1**, **2**, **3** and **4** in CH_2Cl_2 in the region 0.2–0.7 V (*vs.* $[Fc]^+/[Fc]$) are very similar to each other and closely resemble those reported for $[M(^{Ph}L)_2]$ (M = Cu, Zn or Co)[11,15] and $[Co(^{PhOMe}L)_2]$[15]; each compound exhibits two, one-electron, oxidations (Table 3, Fig. 5). Tests for reversibility over the scan rate range 20–300 mV s^{-1} showed that the first oxidation is reversible for **1**, **2** and **4**. Thus, for each of these compounds: (i) ΔE is similar to that of the $[Fc]^+/[Fc]$ couple (Table 3) at all scan rates; (ii) $-i_p^c/i_p^a = 1 \pm 0.1$; and (iii) i_p^a and i_p^c are proportional to (scan rate)$^{1/2}$. These tests could not be performed for **3** because of the significant overlap of the first and second redox processes (Fig. 5(a)). The second one-electron oxidation is reversible for **1** and **2**; however, this is not the case for **4** since the ΔE for this couple is greater than that of the $[Fc]^+/[Fc]$ couple at all scan rates.

The pattern of the potentials observed for the two oxidation processes {$E_{1/2}$ values: (a) $[M(^{Ph}L)_2]$, Co:[15] 0.16 and 0.51; Cu:[11] 0.16 and 0.50; Zn:[11] 0.23 and 0.49 V; (b) $[M(^{PhOMe}L)_2]$, Co:[15] 0.12 and 0.49; Cu: 0.11 and 0.44; Zn: 0.18 and 0.47 V; (c) $[M(^{Bz}L)_2]$, Co:[15] 0.35 and n/a; Cu: 0.36 and 0.58; Zn: 0.41 and 0.48 V} is consistent with each process being ligand-based, with $[M(^{R}L)(^{R}L^{\bullet})]^+$ produced initially and then $[M(^{R}L^{\bullet})]^{2+}$. For **1** and **2**, but not for **3** and **4**, an irreversible reduction process was observed at between −1.5 and −1.8 V (*vs.* Fc^+/Fc). This process may involve the reduction of the Cu(II) centre of **1** and **2** to produce a Cu(I) species.

The potential for the first oxidation of a $[Cu(^{R}L)_2]$ or $[Zn(^{R}L)_2]$ (R = Ph,[11] PhOMe or Bz) complex is significantly less positive than that required for the oxidation of the corresponding ^{R}LH pro-ligand. A similar observation has been reported by Thomas *et al.* for the relative values of the potential required to oxidise a salen-type ligand bound to Cu(II) *vs.* that of the pro-ligand itself.[12] Thus, as observed by these authors, the stabilisation of a phenoxyl radical by coordination to a metal centre is more effective than that provided by hydrogen bonding. The stabilisation provided by bonding to a metal centre such as Cu(II) or Zn(II) could arise, at least in part, due the $M\,d_\pi \rightarrow L\,p_\pi$ back donation being greater for M–$^{\bullet}$OPh than M–$^{-}$OPh. The potential for the $[M(II)(^{R}L)(^{R}L^{\bullet})]^+/[M(II)(^{R}L)_2]$ couple is *ca.* 60 mV lower for Cu(II) than Zn(II) and this additional stabilisation may arise due to spin-pairing between the unpaired electron on the phenoxyl radical and that on the d^9 metal centre. Also, intramolecular $\pi \rightarrow \pi$ interactions may aid the formation of the phenoxyl radical complex, as identified in crystalline $[M(II)(^{Ph}L)(^{Ph}L^{\bullet})][BF_4]$ (M = Cu or Zn);[11] this view is analogous to the proposal that π-stacking of the indole ring of Trp_{290} with Tyr_{272} of GO lowers the potential for oxidation of the latter, noting that mutation of Trp_{290} to His increases the potential by 280 mV.[6]

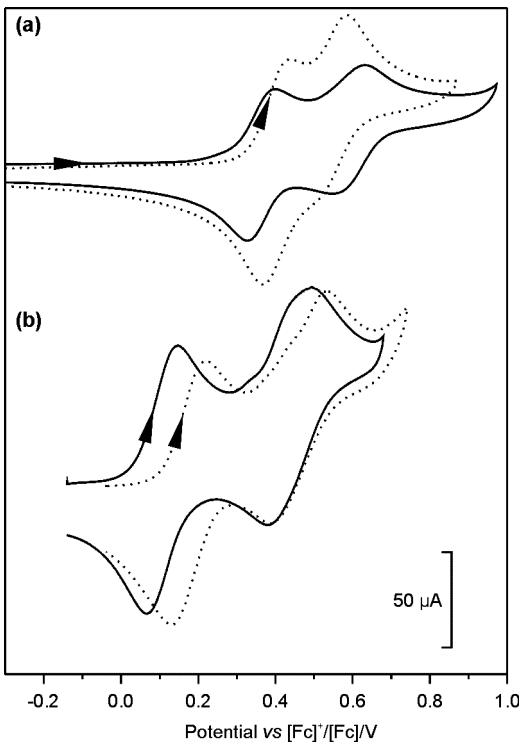

Fig. 5 Cyclic voltammograms of: (a) **1** (—) and **3** (···) and (b) **2** (—) and **4** (···). Data were recorded at a scan rate of 100 mV s^{-1} using a glassy carbon working electrode a *ca.* 1 mM solution in CH_2Cl_2 at 298 K containing $[NBu^n_4][BF_4]$ (0.4 M). The potential is expressed relative to the $[Fc]^+/[Fc]$ couple recorded under the same conditions.

UV/vis and EPR spectra of $[M(^{R}L)(^{R}L^{\bullet})]^+$ (M = Cu or Zn; R = Bz or PhOMe)

The electrochemical, one-electron, oxidation of **1**, **2**, **3** and **4**, at 273 K under N_2 in CH_2Cl_2 containing $[NBu^n_4][BF_4]$ (0.4 M) as the background electrolyte, led a significant colour change in each case: for **1** and **3** an intense, red–pink coloured solution was produced; for **2** and **4** the solution became dark green. The UV/vis spectra, recorded at an OTE, for these oxidations are shown in Fig. 6; in each case, isosbestic points were observed (Table 4). For **1**, **2** and **3** electrochemical reduction of the oxidised species led to

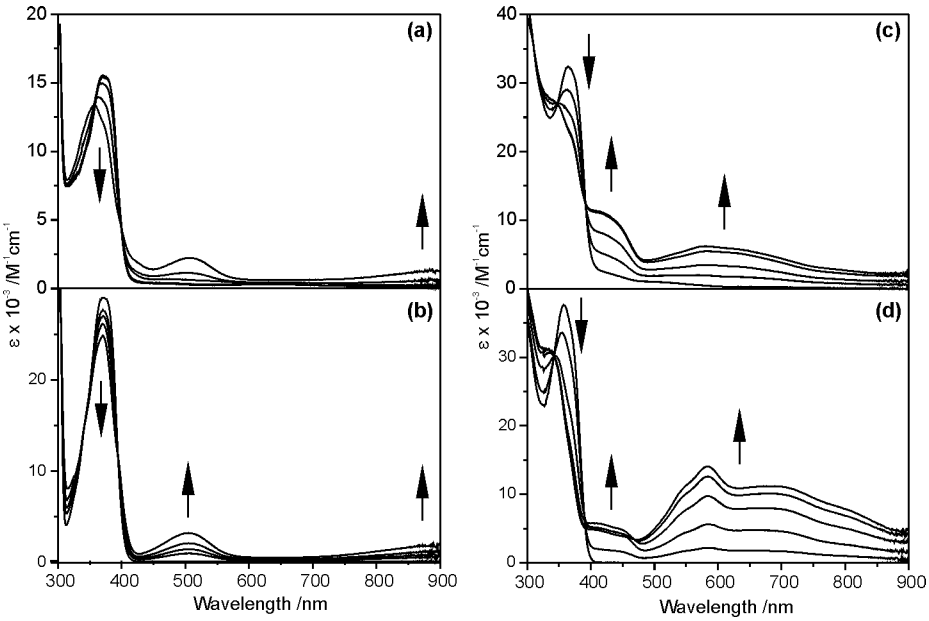

Fig. 6 UV/vis spectra of electrochemically generated $[M(^{R}L)(^{R}L^{\bullet})]^{+}$ (*ca.* 1 mM) in CH_2Cl_2 containing $[NBu^{n}_4][BF_4]$ (0.4 M) in an OTE cell at 273 K: (a) $[\mathbf{1}]^{+}$, M = Cu, R = Bz; (b) $[\mathbf{3}]^{+}$, M = Zn, R = Bz; (c) $[\mathbf{2}]^{+}$, M = Cu, R = PhOMe; (d) $[\mathbf{4}]^{+}$, M = Zn, R = PhOMe.

the UV/vis spectrum of the corresponding $[M(^{R}L)_2]$ compound. Thus, these one-electron electrochemical oxidations are chemically reversible on the timescale of the OTE experiment and produce a single species. However, for **4** the isosbestic point at 390 nm became ill-defined towards the end of the oxidation; this may indicate a time-dependent and/or a concentration-dependent chemical transformation of $[\mathbf{4}]^{+}$ (see Fig. 6(d)). The oxidised solutions of $[\mathbf{1}]^{+}$, $[\mathbf{2}]^{+}$ and $[\mathbf{3}]^{+}$ (*vide infra*) are stable in solution for several hours under the experimental conditions employed.

The UV/vis spectrum of $[\mathbf{2}]^{+}$ and $[\mathbf{4}]^{+}$ (Table 4; Fig. 6(c) and (d), respectively) each contains an absorption at *ca.* 410 nm ($\varepsilon = 11300$ and 5600 M^{-1} cm^{-1}), similar to that observed for the corresponding R = Ph complexes.[11] This absorption is assigned to a $\pi \rightarrow \pi^{*}$ transition of the phenoxyl radical ligand (*vide supra*).[7,8,13,23,28] The corresponding absorption is not clearly manifest in the UV/vis spectra of $[\mathbf{1}]^{+}$ and $[\mathbf{3}]^{+}$ (Table 4; Fig. 6(c) and (d)) and may be masked by the strong band at 360–370 nm. The UV/vis spectrum of $[\mathbf{1}]^{+}$ and $[\mathbf{3}]^{+}$ each possess an absorption at *ca.* 510 nm (*viz.* 506 nm, $\varepsilon = 2300$ M^{-1} cm^{-1}; 508 nm, $\varepsilon = 3200$ M^{-1} cm^{-1}, respectively) similar to that observed for $[Co(III)(^{Bz}L)_2(^{Bz}L^{\bullet})]^{+}$ (503 nm, $\varepsilon = 4420$ M^{-1} cm^{-1})[15] and is assigned to an intraligand charge transfer of $^{Bz}L^{\bullet}$. The UV/vis spectrum of each cation $[\mathbf{1}]^{+}$, $[\mathbf{2}]^{+}$, $[\mathbf{3}]^{+}$ and $[\mathbf{4}]^{+}$ contains broad absorptions between 500 and 900 nm that (*cf.* Fig. 3) are considered to arise from transitions of the phenoxyl radical ligands. Resonance Raman studies, in conjunction with time-dependent DFT-calculations, are in progress to probe the nature of the UV/vis transitions observed of these $[^{R}LH^{\bullet}]^{+}$ and $[M(^{R}L)(^{R}L^{\bullet})]^{+}$ species.

The electrochemical, one-electron, oxidation of **1** and **2** is accompanied by a reduction in the intensity of the EPR signal; *i.e.* $[\mathbf{1}]^{+}$ and $[\mathbf{2}]^{+}$, in CH_2Cl_2 containing $[NBu^{n}_4][BF_4]$ (0.4 M) at 77 K, are essentially EPR silent, only a residual Cu(II) signal, <10% of the intensity of the parent complex, was observed. The lack of an EPR signal for $[\mathbf{1}]^{+}$ and $[\mathbf{2}]^{+}$ is consistent with an $S = 0$ or 1 (with a very large zero-field splitting) ground state, resulting from magnetic coupling between an $S = 1/2$ Cu(II) centre and an $S = 1/2$ coordinated radical ligand, as observed for $[Cu(II)(^{Ph}L)(^{Ph}L^{\bullet})]^{+}$,[11] and other Cu(II)–phenoxyl radical complexes.[28,34]

The EPR spectrum of electrochemically generated $[\mathbf{4}]^{+}$, in CH_2Cl_2 containing $[NBu^{n}_4][BF_4]$ (0.4 M) at 77 K, consists of a single isotropic $S = 1/2$ signal with $g = 2.004$. This *g*-value is within the range of those reported for Zn(II)-phenoxyl radical compounds[33] and is similar to that of $[Zn(II)(^{Ph}L)(^{Ph}L^{\bullet})]^{+}$.[11] The X-band EPR spectrum of $[\mathbf{4}]^{+}$ does not exhibit any resolved hyperfine splitting and possess a relatively narrow line width, *ca.* 10 G, suggesting that the unpaired electron is not appreciably localised on the imidazole N-atoms.

The X-band EPR spectrum of the one-electron oxidised solution of **3** recorded at 77 K in CH_2Cl_2, consists of a five-line symmetric pattern centered at $g = 2$ distributed over a 200 G window (Fig. 7). This spectrum cannot be explained on the basis of a single radical signal, even with the incorporation of *g*-value anisotropy and strong hyperfine splitting involving imidazole N-atoms. Furthermore, the relative intensity of the dominant central feature varies according to the sample preparation and the applied potential, indicating that this signal is independent from the other satellite peaks. The spectrum was deconvoluted into two distinct sub-spectra by simulation. A successful simulation of the spectrum was obtained by the combination of an isotropic $S = 1/2$ signal at $g = 2$ corresponding to $[\mathbf{3}]^{+}$ and a spin-triplet resonance ($S = 1$) that gives rise to the symmetric split-line pattern that is assigned[34,35] to $[\mathbf{3}]^{2+}$, *i.e.* $[Zn(II)(^{Bz}L^{\bullet})_2]^{2+}$. The formation of $[\mathbf{3}]^{2+}$ from the disproportionation of $[\mathbf{3}]^{+}$ is expected, given the overlap of the $[\mathbf{3}]^{+}/[\mathbf{3}]$ and $[\mathbf{3}]^{2+}/[\mathbf{3}]^{+}$ couples in the cyclic voltammogram of **3** (Fig. 5). The $S = 1$ resonance contributes 2/3 of the integrated intensity of the EPR spectrum. For simulation of the $S = 1$ signal, we assumed that the exchange coupling (J) between the two phenoxyl radicals is much larger than the Zeeman splitting ($h\nu \approx 0.3$ cm^{-1} at X-band frequency), for which singlet and triplet states

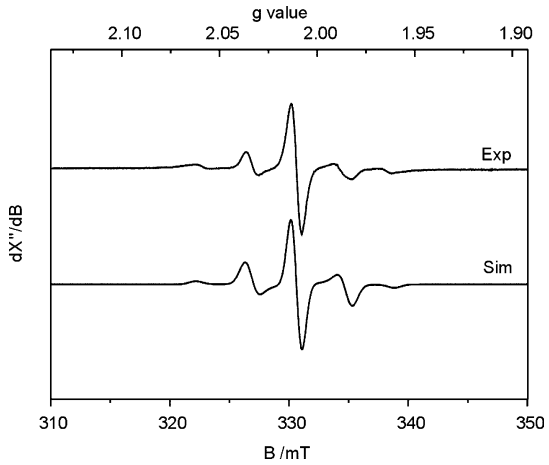

Fig. 7 Upper trace: X-band EPR spectrum recorded for the product (at 175 K; $\nu = 9.27003$ GHz; modulation amplitude = 1 mT; power = 2.01 mW) of the one-electron electrochemical oxidation of **3** (*ca.* 1 mM) in CH_2Cl_2 containing $[NBu^n_4][BF_4]$ (0.4 M); the potential applied was 0.99 V (*vs.* SCE) *i.e.* between the two overlapping oxidation waves (Fig. 5(a)). Lower trace: simulated EPR spectrum: the simulation is the sum of two subspectra I and II in a 1 : 2 ratio, the parameters of which are I: $S = 1$, $g_x = g_y = 2.002$, $g_z = 2.004$, $D = 0.0078$ cm^{-1}, $E = 0$, $W_x = W_y = W_z = 15$ G; II: $S = 1/2$, $g_x = g_y = g_z = 2.000$, $W_x = W_y = W_z = 40$ G.

are well-separated in energy without any significant level mixing. With this assumption, we could simulate the $S = 1$ component as an isolated spin triplet with axial zero-field splitting (ZFS) that arises from the combined effect of intramolecular exchange and spin–dipolar couplings of two radical spins. A successful simulation was obtained with an axial ZFS of $D = 0.0078$ cm^{-1} and $g_{xx} = g_{yy} = 2.002$, $g_{zz} = 2.004$.

Conclusions

This and related studies[10,11,15] have demonstrated that a suitable pro-ligand design, namely one that incorporates *ortho*- and *para*-protection of the phenol and the absence of an oxidisable position (other than the phenolic O–H group), allows a relatively inert phenoxyl radical to be generated, either hydrogen bonded, as in $[^RLH]^{\bullet+}$ or coordinated to a transition metal, as in $[M^{II}(^RL)(^RL^{\bullet})]^+$ (M = Co, Cu or Zn; R = Ph, Bz or PhOMe) complexes. The one-electron oxidation of ^{R}LH (Ph, Bz or PhOMe) is reversible and occurs *via* proton-coupled electron transfer to form $[^RLH]^{\bullet+}$, comprised of a phenoxyl radical hydrogen-bonded to an imidazolium proton. $[M(^RL)_2]$ (M = Co, Cu or Zn; R = Ph, Bz or PhOMe) complexes each undergo two, reversible, one-electron oxidations that are ligand-based; $[M(^RL)(^RL^{\bullet})]^+$ is formed initially and then $[M(^RL^{\bullet})_2]^{2+}$. A phenoxyl radical is stabilised by both hydrogen bonding and coordination to a metal, the latter being more potent than the former and Cu(II) is slightly more effective than Zn(II) in this respect.

References

1 J. Stubbe and W. A. van der Donk, *Chem. Rev.*, 1998, **98**, 705.
2 J. Stubbe, D. G. Nocera, C. S. Yee and M. C. Y. Chang, *Chem. Rev.*, 2003, **103**, 2167.
3 K. E. Silva, T. E. Elgren, L. Que, Jr. and M. T. Stankovich, *Biochemistry*, 1995, **34**, 14093.
4 I. Vass and S. Styring, *Biochemistry*, 1991, **30**, 830.
5 J. W. Whittaker, *Chem. Rev.*, 2003, **103**, 2347.
6 C. Wright and A. G. Sykes, *J. Inorg. Biochem.*, 2001, **85**, 237.
7 T. Maki, Y. Araki, Y. Ishida, O. Onomura and Y. Matsumura, *J. Am. Chem. Soc.*, 2001, **123**, 3371.
8 F. Thomas, O. Jarjayes, H. Jamet, S. Hamman, E. Saint-Aman, C. Duboc and J.-L. Pierre, *Angew. Chem., Int. Ed.*, 2004, **43**, 594.
9 I. J. Rhile and J. M. Mayer, *J. Am. Chem. Soc.*, 2004, **126**, 12718; I. J. Rhile and J. M. Mayer, *Biochim. Biophys. Acta*, 2004, **1655**, 51; I. J. Rhile and J. M. Mayer, *Angew. Chem., Int. Ed.*, 2005, **44**, 1598.
10 L. Benisvy, R. Bittl, E. Bothe, C. D. Garner, J. McMaster, S. Ross, C. Teutloff and F. Neese, *Angew. Chem., Int. Ed.*, 2005, **44**, 5314.
11 (*a*) L. Benisvy, A. J. Blake, D. Collison, E. S. Davies, C. D. Garner, E. J. L. McInnes, J. McMaster, G. Whittaker and C. Wilson, *Chem. Commun.*, 2001, 1824; (*b*) L. Benisvy, A. J. Blake, D. Collison, E. S. Davies, C. D. Garner, E. J. L. McInnes, J. McMaster, G. Whittaker and C. Wilson, *Dalton Trans.*, 2003, 1975.
12 F. Thomas, O. Jarjayes, C. Duboc, C. Philouze, E. Saint-Aman and J.-L. Pierre, *Dalton Trans.*, 2004, 2662.
13 (*a*) B. A. Jazdzewski and W. B. Tolman, *Coord. Chem. Rev.*, 2000, **200-202**, 633; (*b*) S. Itoh, M. Taki and S. Fukuzumi, *Coord. Chem. Rev.*, 2000, **198**, 3; (*c*) P. Chaudhuri and K. Wieghardt, *Prog. Inorg. Chem.*, 2001, **50**, 151.
14 (*a*) F. Thomas, G. Gellon, I. Gautier-Luneau, E. Saint-Aman and J.-L. Pierre, *Angew. Chem., Int. Ed.*, 2002, **41**, 3047; (*b*) A. Philibert, F. Thomas, C. Philouze, S. Hamman, E. Saint-Aman and J.-L. Pierre, *Chem.–Eur. J.*, 2003, **9**, 3803; (*c*) F. Michel, F. Thomas, S. Hamman, E. Saint-Aman, C. Bucher and J.-L. Pierre, *Chem.–Eur. J.*, 2004, **10**, 4115.
15 L. Benisvy, E. Bill, A. J. Blake, D. Collison, E. S. Davies, C. D. Garner, C. I. Guindy, E. J. L. McInnes, G. McArdle, J. McMaster, C. Wilson and J. Wolowska, *Dalton Trans.*, 2004, 3647.
16 J. Cosier and A. M. Glazer, *J. Appl. Crystallogr.*, 1986, **19**, 105.
17 G. M. Sheldrick, SHELX-86–97, *Acta Crystallogr., Sect. A*, 1990, **46**, 467.
18 F. H. Allen, O. Kennard, D. G. Watson, L. Brammer, A. G. Orpen and R. Taylor, *J. Chem. Soc., Perkin Trans. 2*, 1987, S1.
19 C. Foces-Foces, A. L. Llamas-Saiz, R. M. Claramunt, P. Cabildo and J. Elguero, *J. Mol. Struct.*, 1998, **440**, 193.
20 J. Catalán, F. Fabero, M. Soledad Guijarro, R. M. Claramunt, M. D. Santa María, M. C. Foces-Foces, F. Hernández Cano, J. Elguero and R. Sastre, *J. Am. Chem. Soc.*, 1990, **112**, 747.
21 A. L. Llamas-Saiz, C. Foces-Foces, D. Sanz, R. M. Claramunt, J. Dotor, J. Elguero, J. Catalán and J. Carlos del Valle, *J. Chem. Soc., Perkin Trans. 2*, 1995, 1389.
22 M. Lal, A. Langels, H.-J. Deiseroth, J. Schlirf and M. Schmittel, *J. Phys. Org. Chem.*, 2003, **16**, 373.
23 (*a*) E. R. Altwicker, *Chem. Rev.*, 1967, **67**, 475; (*b*) E. J. Land, G. Porter and E. Strachan, *Trans. Faraday Soc.*, 1961, **57**, 1885.
24 (*a*) A. B. Suttie, *Tetrahedron Lett.*, 1969, **12**, 953; (*b*) J. A. Richards, P. E. Whitson and D. H. Evans, *J. Electroanal. Chem.*, 1975, **63**, 311.
25 (*a*) A. Ronlán and V. D. Parker, *J. Chem. Soc. C*, 1971, 3214; (*b*) O. Hammerich in *Organic Electrochemistry*, ed. M. M. Baizer and H. Lund, Marcel Decker, New York, 1983, p. 485.
26 F. G. Bordwell and J.-P. Cheng, *J. Am. Chem. Soc.*, 1991, **113**, 1736.
27 R. H. Holm and M. J. O'Connor, *Prog. Inorg. Chem.*, 1971, **14**, 241.
28 J. A. Halfen, B. A. Jazdzewski, S. Mahapatra, L. M. Berreau, E. C. Wilkinson, L. Que, Jr. and W. B. Tolman, *J. Am. Chem. Soc.*, 1997, **119**, 8217.
29 (*a*) K. D. Karlin, B. I. Cohen, J. C. Hayes, A. Farooq and J. Zubieta, *Inorg. Chem.*, 1987, **26**, 147; (*b*) R. Uma, R. Viswanathan, M. Palaniandavar and M. Lakshminarayanan, *J. Chem. Soc., Dalton Trans.*, 1994, 1219.
30 R. H. Holm, G. W. Everett, Jr. and A. Chakravorty, *Prog. Inorg. Chem.*, 1966, **7**, 83.
31 F. E. Mabbs and D. Collison, *Electron Paramagnetic Resonance of d-Transition Complexes*, Elsevier, Amsterdam, 1992, p. 405.
32 F. E. Mabbs and D. Collison, *Electron Paramagnetic Resonance of d-Transition Complexes*, Elsevier, Amsterdam, 1992, p. 218.
33 J. Peisach and W. E. Blumberg, *Arch. Biochem. Biophys.*, 1974, **165**, 691.
34 E. Bill, J. Müller, T. Weyhermülller and K. Wieghardt, *Inorg. Chem.*, 1999, **38**, 5795.
35 A. Sokolowski, J. Müller, T. Weyhermülller, R. Schnepf, P. Hildebrant, K. Hildenbrand, E. Bothe and K. Wieghardt, *J. Am. Chem. Soc.*, 1997, **119**, 8889.